nature water

Article

https://doi.org/10.1038/s44221-026-00672-3

Global managed aquifer recharge potential as a solution to water scarcity

Received: 9 October 2025

Accepted: 1 June 2026

Published online: 02 July 2026

Check for updates

Andrea Citrini[1], Bridget R. Scanlon[2], Ashraf Rateb[2], Gang Zhao[1,3], Matteo Sangiorgio[4] & Lorenzo Rosa[1]

Groundwater overexploitation from irrigated agriculture is accelerating in major food-producing regions, threatening long-term water and food security. Managed aquifer recharge (MAR), the intentional storage of available water in aquifers, could help buffer hydrologic extremes by diverting high flows for infiltration. Here we present a first-order global screening of spreading-based MAR potential across irrigated lands (2002–2021) by integrating Gravity Recovery and Climate Experiment-derived monthly groundwater depletion, high-magnitude flow and unsustainable irrigation water consumption. We estimate high-magnitude flow volumes under 90th and 95th percentile thresholds and weight them with a region-/monthly-specific feasibility coefficient representing infiltration suitability, evaporative competition and off-season crop-area availability. Globally, MAR could offset 4–6% of unsustainable irrigation, with hotspots reaching more than 50% offset (for example, Europe and Southeast Asia) but lower potential in basins such as the Ganges and the Central Valley (3–7%). Our results warrant subsequent regional assessments to evaluate technical, economic and governance/policy feasibility, as well as site-specific design.

Irrigated agriculture accounts for 90% of global freshwater consumption and plays a key role in food production[1]. By providing a controlled water supply, irrigation reduces the impacts of droughts, heat stress and rainfall variability, making it essential for maintaining agricultural productivity and food security in a changing climate[2].

Globally, 40% of irrigation relies on groundwater[3], particularly in semi-arid and arid regions, where surface water is scarce and erratic[4]. Nearly half of the irrigation water consumption is unsustainable, exceeding local recharge rates and leading to aquifer depletion, reduced streamflow and ecosystem degradation via environmental-flow depletion[5].

Data from the Gravity Recovery and Climate Experiment (GRACE) and its Follow-On (FO) mission have transformed global groundwater monitoring, revealing important declines in critical aquifers[6,7]. These losses impair environmental-flow requirements, accelerate land subsidence and intensify competition for water among agricultural, urban and industrial users[8,9].

Addressing water scarcity requires action in two directions: increasing water availability and/or demand management by focusing on improving irrigation efficiency and selecting less water-intensive crops[10]. Increasing water availability involves enhancing storage capacity[11,12], wastewater reuse[13,14] and desalination[15]. Additional approaches include inter-basin water transfers[16], virtual water trade[17] and extracting moisture from the atmosphere[18]. Only the combined and regionally adapted application of these solutions can safeguard water security[19].

Managed aquifer recharge (MAR) represents a strategy to address groundwater depletion by actively replenishing aquifers using available

[1]Biosphere Sciences and Engineering, Carnegie Institution for Science, Stanford, CA, USA. [2]Bureau of Economic Geology, Jackson School of Geosciences, University of Texas at Austin, Austin, TX, USA. [3]Key Laboratory of Water Cycle and Related Land Surface Processes, Institute of Geographic Sciences and Natural Resources Research, Chinese Academy of Sciences, Beijing, China. [4]Department of Electronics, Information and Bioengineering, Politecnico di Milano, Milan, Italy. e-mail: lrosa@carnegiescience.edu

water[20,21]. MAR can help offset unsustainable irrigation by capturing excess floodwater for infiltration into depleted aquifers while enhancing the conjunctive surface and groundwater management[22–25]. Despite the growing recognition of MAR as a viable groundwater management strategy, its potential remains under-utilized, contributing only 1% (10 $km^3\ yr^{-1}$) of global groundwater extraction[20]. Previous studies have predominantly examined MAR at regional or site-specific scales without extending the analysis worldwide[26]. Moreover, global analyses have not integrated the key factors for prioritizing MAR in irrigated agricultural regions, such as the co-occurrence of high-magnitude surface flows, long-term groundwater depletion and unsustainable irrigation. This leaves a critical gap in understanding where MAR could be most effectively deployed to address irrigation-induced water scarcity, as well as the constraints and opportunities on a global scale for prioritizing investments and driving site-specific studies, where MAR could yield the highest benefit.

We present a global-scale assessment of MAR spreading potential by integrating two decades of GRACE-based groundwater depletion, high-magnitude flow (HMF) estimates, region- and monthly-specific feasibility constraints and unsustainable irrigation water consumption (Supplementary Fig. 1). MAR spreading is a technique that intentionally diverts excess surface water, such as floodwater or stormwater, over permeable land, infiltration basins or recharge ponds, to seep through the soil and replenish unconfined aquifers. We first characterize global patterns of groundwater depletion in irrigation regions from monthly GRACE-derived groundwater storage (GWS) anomalies (2002–2021). We then quantify the potential for MAR to mitigate unsustainable irrigation by estimating feasibility-weighted, above-threshold HMF volumes (90th and 95th percentile thresholds) and benchmarking them against region-specific depletion and unsustainable irrigation demand. We further evaluate sensitivity to different HMF capture efficiencies and assess interannual variability in MAR potential to identify years and regions where offset responds strongly to extreme-flow conditions.

This study offers a first-order, global screening of MAR feasibility to support strategic prioritization at the basin-to-national scale. While not a substitute for site-specific design and permitting, the results flag where and when MAR may merit targeted local assessments by water managers under climate extremes, motivating subsequent site-specific studies to evaluate feasibility and design. These findings can help guide surface water and groundwater management strategies, enhancing the potential for irrigated agriculture to adapt to climate extremes while safeguarding long-term water security.

Results

Global patterns of groundwater depletion in irrigation regions

Groundwater trends obtained on the basis of the residual method[27] from the GRACE (-FO) missions revealed widespread groundwater depletion across major global irrigation regions between April 2002 and December 2021 (Figs. 1 and 2). We quantified long-term groundwater changes, using the GRACE (-FO) total water storage (TWS) anomalies, relative to the long-term mean (2002–2021). TWS is assumed to represent the sum of water stored in a region, including groundwater, soil moisture, snow and surface water[28]. To isolate GWS anomalies, we subtracted the contributions of soil moisture, snow and surface water by using land surface models and observational datasets (Methods). Time series for ten highly impacted regions show consistent downward trends in GWS (Fig. 2). All values include Theil–Sen trend uncertainties (2002–2021) (Methods). The Ganges River Basin shows the largest absolute loss of GWS, with a trend of −16.4 mm yr^{-1}, corresponding to a cumulative depletion of 283.9 ± 49.0 km^3 (2002–2021) (Figs. 1 and 2a). Other river basins also exhibit substantial rates of groundwater depletion, such as the Sabarmati River (−14.8 mm yr^{-1}, 83.8 ± 22.3 km^3), the Ziya River (−18.7 mm yr^{-1}, 73.8 ± 9.2 km^3), the Lower Yellow River (−11.6 mm yr^{-1}, 42.6 ± 4.0 km^3) and the Indus River (−6.9 mm yr^{-1}, 36.6 ± 8.6 km^3) (Fig. 2b–e). Several regions in eastern Europe, parts of Southeast Asia and southern South America display gains in GWS, with some exceeding 10 km^3 in 2002–2021, namely, the Lower Yangtze River (27.8 ± 7.7 km^3), the Upper Yangtze River (17.2 ± 5.2 km^3), the Godavari River (16.4 ± 11.3 km^3), the Pearl River (8.8 ± 5.7 km^3) and the Mahanadi River (8.6 ± 11.3 km^3) (Fig. 1). These gains may reflect reduced irrigation demand, supplemental surface-water supplies, stronger groundwater management and regulation, and/or favourable recharge conditions.

Together, these contrasting trends underscore the spatial heterogeneity of groundwater dynamics in irrigated systems worldwide. While depletion remains widespread in some breadbaskets, isolated gains offer critical insights into conditions that enable groundwater stabilization. These patterns help identify high-risk and high-opportunity regions for groundwater sustainability, including MAR.

Potential of MAR to mitigate unsustainable irrigation

The capacity of MAR to alleviate unsustainable irrigation varies substantially worldwide, reflecting the spatial heterogeneity in both surface water availability and groundwater depletion (Fig. 3). We estimate this capacity by converting HMF volumes screened for environmental flow requirements (EFRs) into a potential offset of unsustainable irrigation, after down-weighting by the region- and monthly-specific feasibility coefficient $M(r, t)$ (Methods, equations (2) and (3), and Extended Data Fig. 1).

The results reveal a gradient of feasibility, with high MAR potential in South Asia, Central Europe and parts of Central and South America (Fig. 3). In some important irrigation regions, MAR could compensate a fraction of unsustainable irrigation, such as 3–7% in the Ganges River, 3–6% in California Central Valley, 4–7% in the Lower Yellow River, 11–25% in the Upper Yellow River, 2–4% in the Ziya River, 3–6% in the Nile Delta, 16–23% in the Upper Tigris–Euphrates and 15–22% in the Lower Tigris–Euphrates considering the 95th and 90th percentile HMF scenarios, respectively (Fig. 3). To help interpret these region-level differences, we examined two period-integrated constraint diagnostics (Supplementary Fig. 2 and Supplementary Text 1). The Ganges River, Lower Yellow River and Ziya River remain HMF-supply constrained under both percentile scenarios, whereas the California Central Valley and Upper Yellow River shift from depletion-cap constrained at the 90th percentile to HMF-supply constrained at the 95th percentile; the Nile Delta and the Upper and Lower Tigris–Euphrates remain depletion-cap constrained in both cases. Low offsets in the Ganges River, California Central Valley, Lower Yellow River, Ziya River and Nile Delta are further associated with strong irrigation consumption pressure relative to the maximum bankable recharge volume, whereas the larger offsets in the Upper Yellow River and the Upper and Lower Tigris–Euphrates are consistent with lower irrigation consumption pressure.

Regions shaded in deep blue, such as the central European regions, Southeast Asia, parts of the Central and Southwest America, Japan and Madagascar, exhibit MAR offset potentials exceeding 80% under both the 90th and 95th percentile HMF scenarios (Fig. 3a). These high-offset regions are generally associated with depletion-cap constraint and lower irrigation consumption pressure, consistent with cumulative feasible HMF supply being sufficient to approach the selected restoration target in both scenarios (Supplementary Fig. 2 and Supplementary Text 1). These areas represent prime candidates for strategic recharge interventions as they combine high groundwater depletion with surface water surpluses. Conversely, many irrigation regions in Sub-Saharan Africa and Central Asia, the Indian subcontinent, the Mediterranean region and parts of western North and Central America show limited MAR feasibility (<20%) (Fig. 3a). Across regions, these low offsets reflect different combinations of HMF-supply constraint, depletion-cap constraint and irrigation consumption pressure, while local factors not resolved here must be assessed in subsequent site-scale studies. Figure 3b shows the differences between optimistic (90th percentile) and conservative (95th percentile) recharge scenarios. This contrast is especially pronounced in parts of South Asia, the Middle East, Central

https://doi.org/10.1038/s44221-026-00672-3

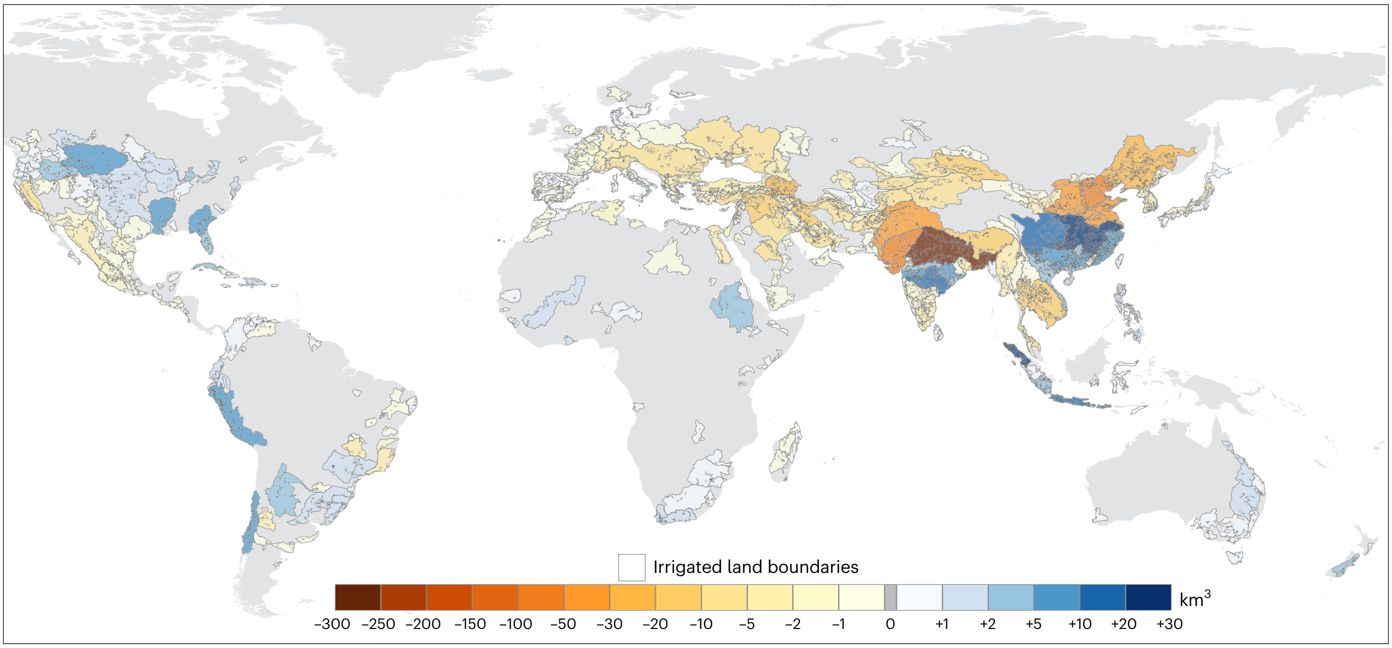

Fig. 1 | Global net GWS volume change in irrigation regions, 2002–2021. Net GWS volume change (cubic kilometres) in irrigation regions between April 2002 and December 2021, derived from GRACE (-FO) data. Irrigation regions are coloured according to GWS change, with warmer colours indicating groundwater loss and cooler colours indicating groundwater gain. Black-outlined polygons show irrigated land boundaries within each irrigation region. Basemap data from Esri, Garmin International, Inc., the US Central Intelligence Agency (The World Factbook) and the National Geographic Society.

Asia and Central Europe, where the percentage of unsustainable irrigation offset by MAR drops by around 30–45% over the 2002–2021 period under the conservative HMF scenario, substantially lower than the values exceeding 70% observed in the more optimistic scenario for regions such as the Danube River (Central Europe), the Lower Volga River (Russia–Kazakhstan), the Irrawaddy River (Myanmar) and the Chao Phraya River (Thailand) (Fig. 3b). These reductions reflect strong hydrological variability, with recharge opportunities concentrated in relatively few extreme flow events (Supplementary Fig. 3), highlighting the need for highly adaptive and flexible MAR infrastructure in these areas.

Sensitivity to different HMF capture efficiencies

We benchmarked the region-specific feasibility scenario against uniform HMF capture efficiencies of 100% (namely, capturing all HMF), 50% and 10% under both the 90th and 95th percentile thresholds (Extended Data Fig. 2). Figure 4 shows the feasibility-weighted percentage of unsustainable irrigation water consumption offset by MAR (90th in blue and 95th in orange). Overlaid are the outcomes for uniform 100% (grey bar extent), 50% (solid line) and 10% (dotted line), thereby enabling identification of the equivalent uniform efficiency for the global case and for the top 20 irrigation regions with the highest MAR potential.

In most regions, the feasibility-weighted offset of unsustainable irrigation water consumption by MAR lies well below the uniform 100% reference (grey bar) and typically between the 10% and 50% uniform cases (dotted and solid lines). A few systems retain comparatively high offsets: the Danube River shows 88% (90th) dropping to 57% (95th), that is, a 31% sensitivity to the HMF threshold; Chao Phraya reaches 85% (90th) but falls to 40% (95th; 45% drop); the Mekong Delta declines from 57% (90th) to 33% (95th; 24%), and the Lower/Upper Tigris–Euphrates register 22%/23% at the 90th against 15%/16% at the 95th. By contrast, many large irrigation regions sit at or below an equivalent uniform efficiency of ~10% even under the 90th-percentile HMF threshold, including the Ganges River, the Lower Yellow River, the Manchurian Plains, the Huai River, the California Central Valley, the Indus River, the Ziya River, the Junggar Basin and the Sabarmati River, where the move to the 95th percentile suppresses offsets further. Aggregating globally, the feasibility-weighted MAR offset remains single-digit, from 6% (90th) to 4% (95th), underscoring that once operational constraints are accounted for, many regions behave as ≤10% uniform-efficiency systems, while only a smaller subset consistently exceeds 10% and, in a few cases, approaches ~50%.

Interannual variability in MAR potential

To further explore the spatiotemporal dynamics of MAR feasibility at the interannual level, we assessed the annual percentage of unsustainable irrigation that could be offset by MAR across the 20 most groundwater-stressed irrigation regions over the 2002–2021 period on the basis of GRACE (-FO) (Fig. 5). The heat map illustrates striking heterogeneity across regions, scenarios and through time, revealing distinct patterns of MAR potential aligned with HMF availability and unsustainable irrigation.

Several irrigated regions reach full offset in multiple years under the 90th-percentile HMF scenario, whereas under the 95th percentile threshold, they (at times) fail to attain meaningful offsets, revealing a step-like limit imposed by the smaller volumes available for infiltration. This behaviour is evident in the Chao Phraya River, the Mekong Delta, the Danube River, the Upper and Lower Tigris–Euphrates, and along the Persian Gulf coast, with offsets generally increasing towards the end of the study period, consistent with more frequent and larger above-threshold exceedances that increase the cumulative HMF, driven by increasing extreme rainfall and flooding events[29]. Notably, the Brahmaputra River displays sustained 100% coverage across all years, indicating persistent alignment between surplus surface water and modelled demand (Fig. 5). By contrast, regions such as the Huai River, the Manchurian Plains, the Iran Central Plateau, the Khorasan Plateau, and the California Central Valley show substantial interannual variability, with coverage ranging from 0% in dry years to >40% during periods of elevated HMF availability (Fig. 5). The Ganges River, the Ziya River, the Kura-Aras Basin, the Tarim River, the Junggar Basin and the Lower Yellow River are emblematic cases in which feasibility constraints sharply limit performance: under the 90th-percentile HMF scenario,

https://doi.org/10.1038/s44221-026-00672-3

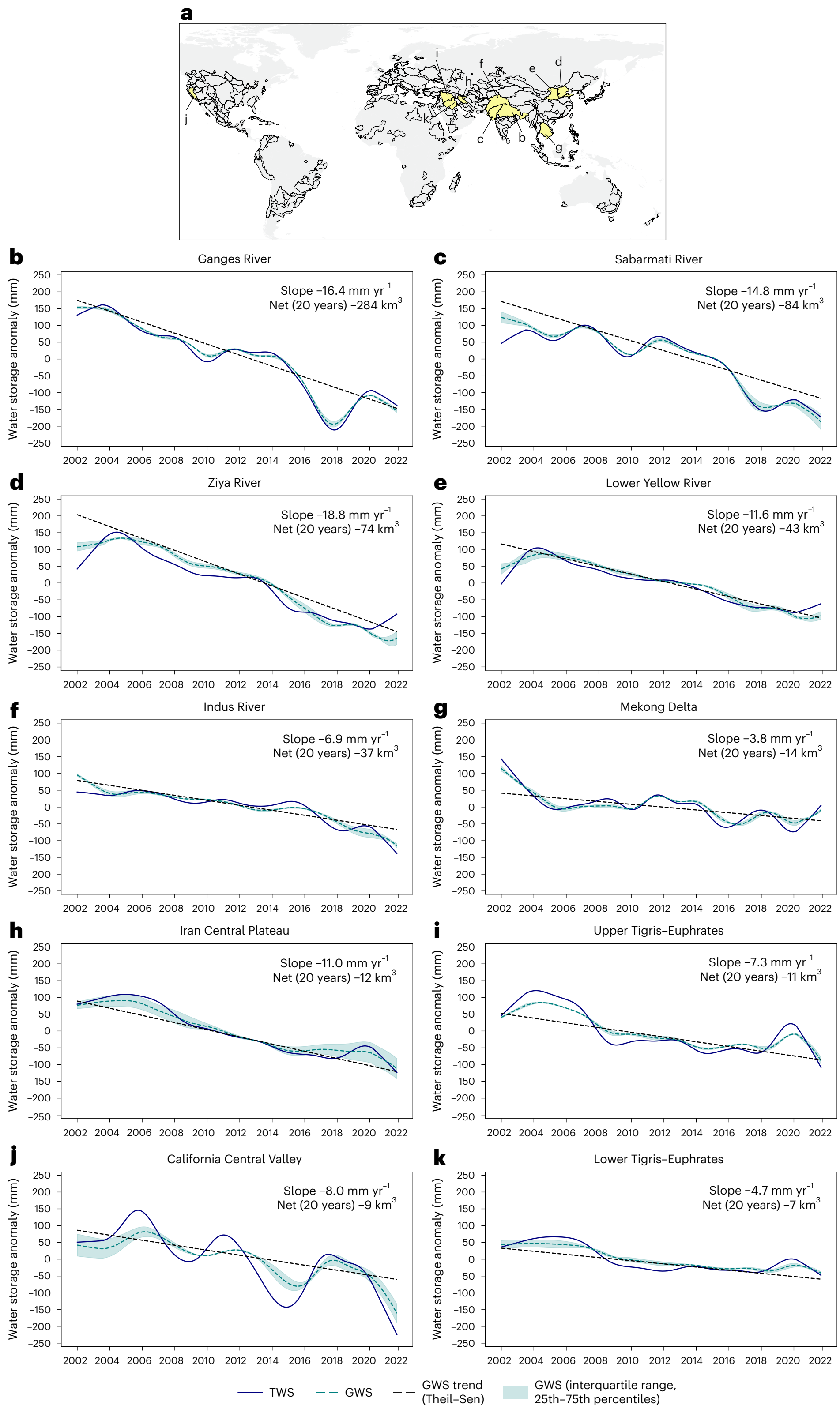

Fig. 2 | GWS anomalies in selected irrigation regions, 2002–2021. a, A global map showing the location of the ten irrigation regions analysed. **b**–**k**, Long-term variability of TWS and GWS over 20 years in major irrigation regions heavily affected by groundwater depletion: Ganges River (**b**), Sabarmati River (**c**), Ziya River (**d**), Lower Yellow River (**e**), Indus River (**f**), Mekong Delta (**g**), Iran Central Plateau (**h**), Upper Tigris–Euphrates (**i**), California Central Valley (**j**) and Lower Tigris–Euphrates (**k**). Reported slopes indicate the annual rate of groundwater depletion (in millimetres per year), while net values represent the total cumulative groundwater loss (in cubic kilometres) over the 2002–2021 period. Lines show median values, shaded bands indicate the interquartile range (25th–75th percentiles) of GWS across the ensemble combinations of GRACE (CSR, Center for Space Research; JPL, Jet Propulsion Laboratory) and GLDAS sources (Noah and VIC). Basemap data in **a** from Esri, Garmin International, Inc., the US Central Intelligence Agency (The World Factbook) and the National Geographic Society.

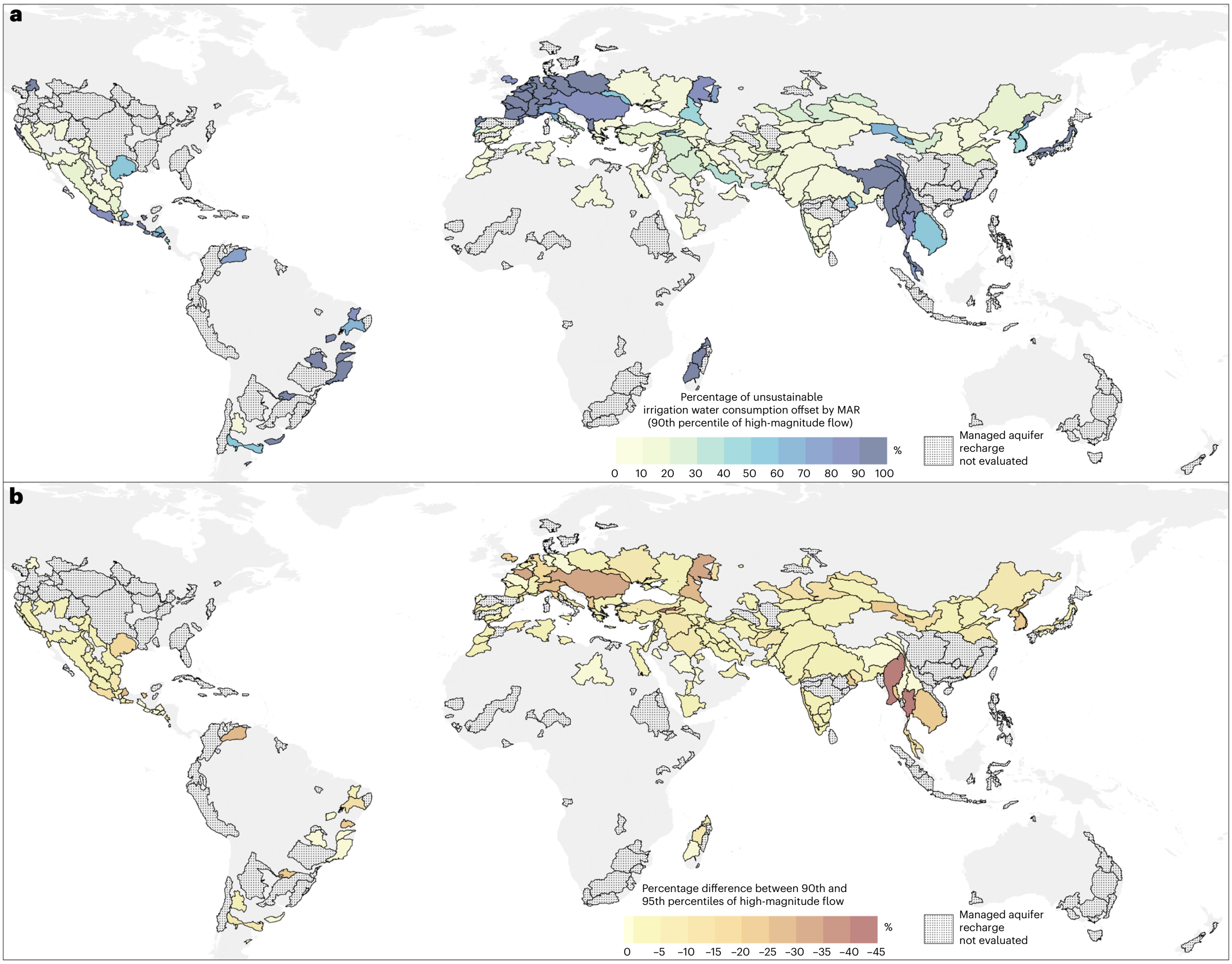

Fig. 3 | Potential of MAR to offset unsustainable irrigation and its sensitivity to the HMF threshold definition. a, The percentage of unsustainable irrigation that could be offset by MAR from 2002 to 2021, assuming the utilization of HMF, defined as the cumulative volume of flow events exceeding the 90th-percentile threshold, after pre-scaling HMF volumes by a region- and monthly-specific feasibility coefficient. Lighter colours indicate lower offset potential, whereas darker blue colours indicate higher offset potential. **b**, The percentage difference of HMFs between the 90th and 95th percentile exceedance-threshold scenarios, computed with the same feasibility weighting, indicating the sensitivity of MAR potential to the definition of HMF thresholds. Colours closer to 0 indicate smaller differences between scenarios, whereas darker orange–brown colours indicate larger reductions under the more conservative 95th percentile scenario. Areas where MAR was not evaluated are presented with grey hatching (modelled unsustainable irrigation water consumption of 0 and/or median GRACE-inferred groundwater depletion over 2002–2021 ≤0 within the irrigation region). Basemap data from Esri, Garmin International, Inc., the US Central Intelligence Agency (The World Factbook) and the National Geographic Society.

the percentage of unsustainable irrigation water consumption offset exceeds 10% in fewer than half of the study years. In the Ganges, for example, exceedances occur only in 2006–2007 and 2010–2011. Moreover, the spread of values under the two HMF scenarios varies from year to year, illustrating the interannual variability of MAR potential under different HMF availability conditions (Fig. 5). Regions such as the Sabarmati River and the Indus River exhibit low MAR effectiveness across most years, reflecting either limited surplus surface water or low estimated aquifer storage availability based on groundwater depletion trends (Fig. 4). These fluctuations underscore the importance of seasonally adaptive MAR planning that aligns recharge operations with hydrologic windows of opportunity.

Taken together, these results underscore the importance of flexible MAR strategies that account for hydrological variability and site-specific hydrogeological constraints. This analysis also reinforces the need to align infrastructure, policy and environmental-flow requirements to enable recharge during episodic HMF periods, thereby maximizing the contribution of MAR to irrigation sustainability.

Discussion

Our findings confirm that MAR can play a valuable role in sustaining agricultural production in water-scarce regions by harnessing HMFs to replenish overexploited aquifers. We demonstrated that MAR potential is spatially heterogeneous and strongly governed by the interaction of three primary factors: (1) the magnitude and frequency of available surface water flows, (2) the volumetric storage capacity of depleted aquifers and (3) the scale of unsustainable irrigation. In addition, region-specific feasibility controls (captured by the coefficient *M*) further constrain capture by down-weighting HMF volumes before MAR (infiltration suitability, seasonal evaporative competition, cold-season suppression and off-season crop-area availability), and in many irrigation regions these feasibility terms are as or more

https://doi.org/10.1038/s44221-026-00672-3

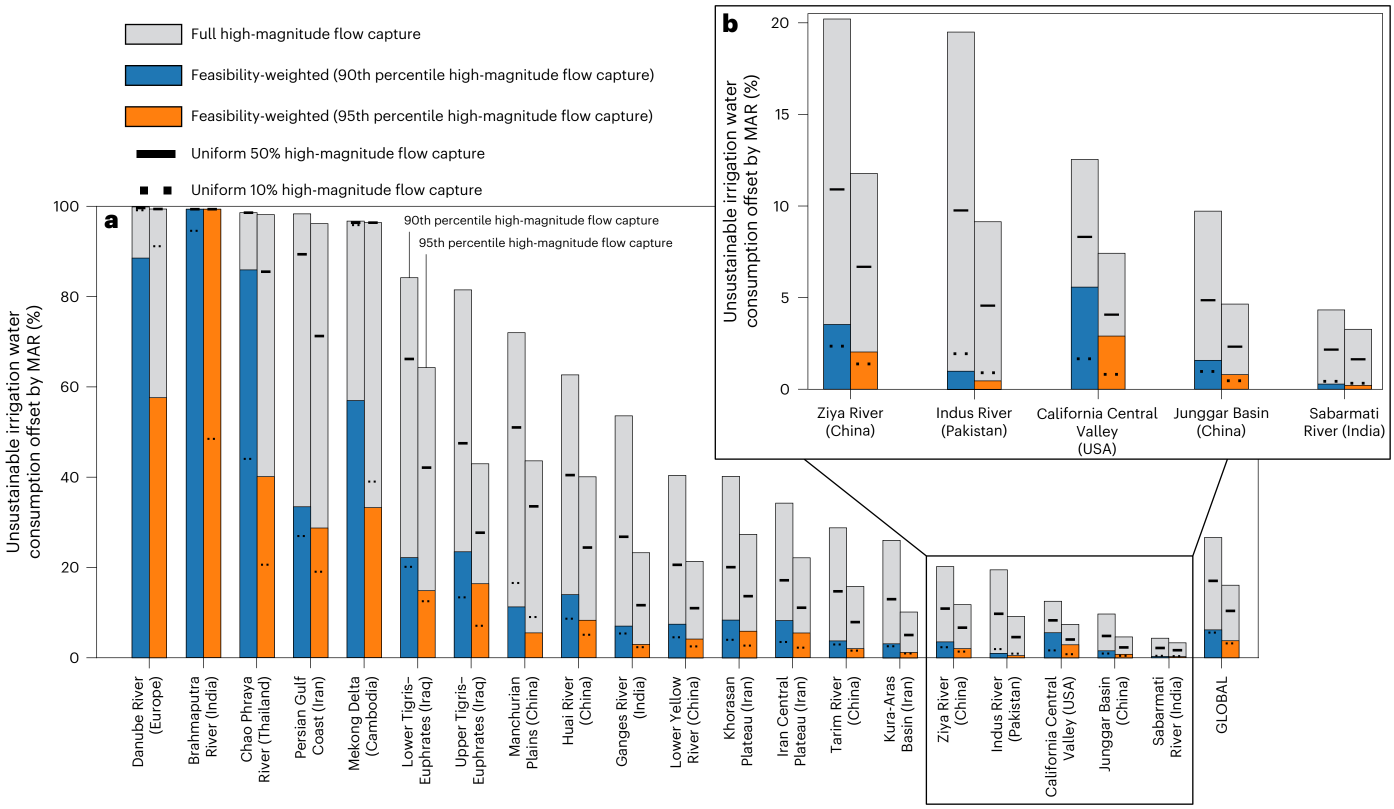

Fig. 4 | Sensitivity of MAR offset potential to different HMF capture-efficiency assumptions. **a**, For selected irrigation regions, bars show the feasibility-weighted percentage of unsustainable irrigation water consumption offset by MAR under the 90th (blue) and 95th percentile (orange) HMF thresholds. The grey bars represent the percentage offset under the 100% uniform HMF capture-efficiency scenario, while horizontal markers denote the outcomes under 50% (solid) and 10% (dotted) uniform capture efficiencies. **b**, An expanded view of low-offset regions, showing irrigation regions where the feasibility-weighted unsustainable irrigation water consumption offset is <20% in the 90th percentile case.

limiting than storage or flow magnitude (Fig. 4). Where surface-water availability constrains these high-flow recharge opportunities, MAR could still be complemented by alternative water sources (for example, treated wastewater recharge[30], transfers/conveyance[31], desalination[32], reservoir re-operations[33] or stormwater capture[34]), which are not evaluated here. This framework aligns with recent modelling efforts in the California Central Valley, where simulation-optimization approaches demonstrate that targeted MAR infrastructure could cost-effectively recover large groundwater volumes[24]. Previous global screening efforts, such as the Underground Transfer of Floods for Irrigation global suitability assessment, mapped potential flood-to-aquifer opportunities using a weighted overlay of flood/drought hazard proxies and broad hydrogeologic indicators (for example, groundwater depth, aquifer type and salinity) to identify co-location of depletion and high suitability[35]. Several hotspots highlighted in our study have already been investigated in basin-scale MAR/Underground Transfer of Floods for Irrigation assessments (for example, the Ganges suitability mapping and large-scale MAR modelling in the North China Plain), and our contribution is to place these results into a single, globally consistent, time-resolved framework that enables cross-basin comparability and prioritization[36,37].

Our results highlight that surface flows exceeding environmental-flow requirements, particularly those above the 90th and 95th percentile scenarios, constitute a largely unused recharge opportunity. This finding aligns with the findings of Kocis and Dahlke[23], who demonstrated that episodic high flows in California could support extensive groundwater banking when strategically managed.

Consistent with the strong spatial heterogeneity identified by our framework, the extent to which these excess flows can be converted into recharge varies widely across regions. In the Po Valley (Italy) (Supplementary Figs. 4 and 5), we find that a modest unsustainable irrigation, with maximum peaks around 1 km^3 yr^{-1} over two decades, could be fully offset through MAR, with depleted aquifer storage (~5 km^3) offering ample space to accommodate MAR recharge potential. These findings expand on the study by Carlson et al.[38], who show that irrigation inefficiencies have historically supported unintentional recharge, particularly in the upper plains fed by alpine runoff. Our results suggest that implementing this recharge through MAR could stabilize declining trends in the lower and central plains, enhancing resilience without compromising ecological flows. In the Ganges River Basin, we estimate ~284 km^3 of groundwater loss between 2002 and 2021, making it the most depleted irrigation region globally. This estimate aligns with Dangar and Mishra[39], who reported ~227 km^3 of GWS loss from 2002–2016. In addition, Panda et al.[40] identified annual GWS losses as high as 189 km^3 in specific sub-regions of northern India, highlighting the intensity of local depletion rather than a basin-wide total in the 2003–2015 period. Their observations of declining groundwater contributions to the Ganges River provide a process-based explanation for the depletion trends our GRACE-based estimates confirm. In California's Central Valley, we estimate a depletion of ~9 km^3 from 2002 to 2021, lower than long-term estimates by Scanlon et al.[41,42], who reported ~80 km^3 lost from the 1960s to 2010. More recent work by Liu et al.[43] reported a loss of ~44.3 ± 0.9 km^3 between 2003 and 2021. Our relatively lower estimate probably reflects both improved recharge efforts and conservative assumptions under our global framework, and potential differences in the time periods considered. Still, the Central Valley remains a prime example of successful MAR integration, where engineered systems have demonstrated the capacity to stabilize aquifer trends[41]. Our feasibility-weighted screen indicates ~6% unsustainable irrigation offset in the California Central Valley

https://doi.org/10.1038/s44221-026-00672-3

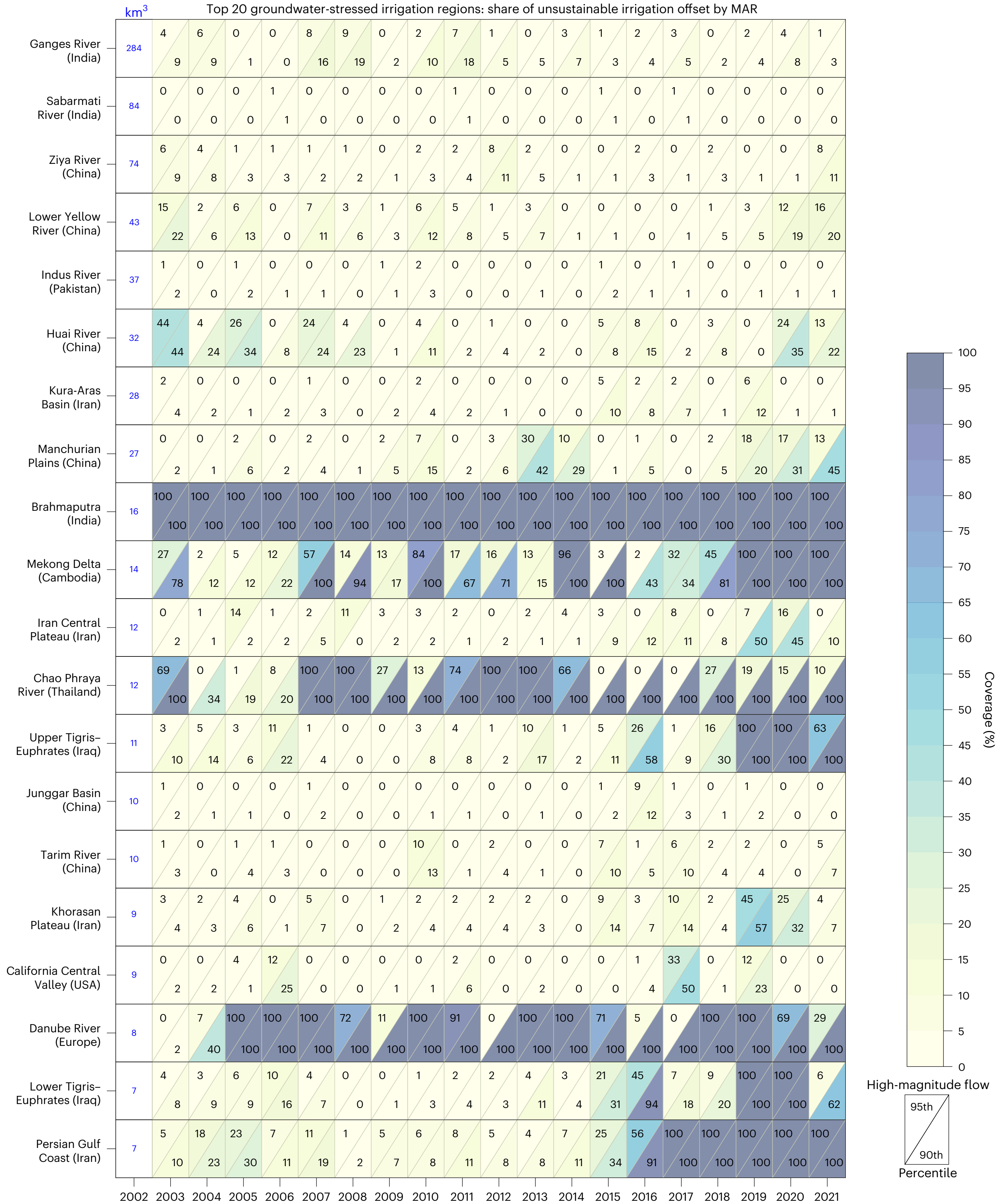

Fig. 5 | Interannual share of unsustainable irrigation offset by MAR for the top 20 irrigation regions affected by groundwater depletion, 2002–2021. A heat map showing the percentage of unsustainable irrigation covered by MAR for the top 20 most groundwater-stressed irrigation regions from 2002 to 2021. Each cell displays triangular coverage values for the 90th (lower right) and 95th (upper left) percentile scenarios. Lighter colours indicate lower coverage, whereas darker blue colours indicate higher coverage, reaching 100% where MAR fully offsets modelled unsustainable irrigation water consumption. Cumulative groundwater depletion volumes for 2002–2021 (in cubic kilometres) are indicated in the leftmost column. Values indicate the proportion of unsustainable irrigation water consumption that could be sustainably met through MAR, highlighting the spatial and temporal variability in MAR feasibility and potential.

(90th percentile, 2002–2021), consistent with a seasonal buffering role in wet years rather than sustained aquifer recovery. Alam et al.[31] report 9–22% overdraft recovery for the Central Valley as a whole, rising to ~30–62% in southern sub-basins with engineered transfers: a difference arising from the metric, space–time resolution and assumptions. The two results are complementary, addressing different decision contexts (strategic screening versus regional design). Finally, in the Danube Basin, we estimate ~8 km^3 of cumulative depletion, consistent with regional studies. Farkas et al.[44] observed 7–8 km^3 of groundwater loss in Hungary's southern Great Plain. These patterns indicate that groundwater overuse is not confined to arid regions but also affects temperate zones with climatic water imbalances and high irrigation demands.

These results should be interpreted as a first-order global screening of hydrologic opportunity rather than as implementable recharge volumes. The MAR scenario assumes idealized recharge and extraction, spatially uniform infiltration behaviour within irrigation regions and no explicit land-use, infrastructure, permitting or policy constraints. To partly reflect operational limitations, we pre-scale HMF volumes using the region- and monthly-specific feasibility coefficient M and benchmark the feasibility-weighted results against uniform capture-efficiency scenarios of 100%, 50% and 10% under both the 90th and 95th percentile HMF thresholds (Fig. 4 and Extended Data Fig. 2). We also cap recoverable storage at cumulative GRACE-derived depletion over 2002–2021, which provides a consistent restoration target and an internally comparable upper bound on MAR feasibility across regions, but may be conservative in some high-capacity systems and restrictive in others. Under this rule, the High Plains appears out of scope in Fig. 3 because the ensemble-median net GWS change within the irrigated-region footprint is slightly positive (+1.2 km^3), which yields a zero storage cap, although the associated uncertainty is large (±15.4 km^3, as a semi-amplitude of the 95% confidence interval). This reflects the analysis window and spatial aggregation adopted here and should not be interpreted as a judgement on local MAR feasibility, which requires basin- and site-specific assessment.

Real-world MAR performance may therefore differ from our screening estimates because the framework does not explicitly resolve site clogging, aquifer heterogeneity, uncertain infiltration rates, interference with other groundwater uses, shallow water-table rise, salinity, contamination, sediment loading, reservoir regulation or conveyance operations, all of which can materially alter realizable recharge volumes and may require pretreatment, adaptive diversion rules and risk-based management[20,21,45]. Economic and institutional feasibility are equally important: although infiltration/spreading approaches using untreated water are often among the lower-cost MAR options, well-based recharge, major conveyance works and advanced treatment can be substantially more expensive[46], while weak governance, inadequate environmental-flow protection and contested water rights may constrain implementation[8,47,48]. Because the modelled unsustainable irrigation is source-agnostic, the estimated offsets should be interpreted as reductions in irrigation stress rather than as direct groundwater savings in every setting; intersecting irrigation regions with a groundwater-share map provides useful context in this regard (Supplementary Fig. 6). MAR is therefore best viewed as one component of broader adaptation portfolios, consistent with recent evidence that groundwater recovery often depends on combinations of alternative water supplies, policy or market interventions and artificial recharge[49].

Our feasibility-weighted global screening of HMFs coincident with depleted aquifers indicates that MAR can provide a limited yet policy-relevant reduction of unsustainable irrigation in hydrologically favourable regions and seasons, best pursued as part of a broader portfolio to enhance groundwater sustainability. MAR offers an adaptive tool to increase water resilience under increasing climate extremes and demographic pressures by leveraging hydrologic variability and available aquifer storage. However, aiming towards its full potential requires more detailed regional scale analysis that integrates planning, robust governance and sustained investment in both physical and institutional infrastructure.

Methods

Summary

We developed a global-scale assessment framework to quantify the potential of MAR to offset groundwater depletion and mitigate unsustainable irrigation (Supplementary Fig. 1). Recognizing the dual challenge of declining groundwater reserves and increasing irrigation demand, we integrated three core components: (1) two decades of satellite-derived GWS anomaly data to detect long-term depletion trends, (2) estimates of HMF availability suitable for MAR operations and (3) an intra-annual water balance-based quantification of unsustainable irrigation. To evaluate the effectiveness of MAR, we constructed a MAR-scenario in which surplus surface water is captured and recharged, contrasting with observed conditions without MAR application, allowing us to estimate the fraction of unsustainable irrigation that could have been resolved over the 2002–2021 period. This spatially explicit, temporally resolved analysis enables the identification of priority regions where MAR implementation could have the most pronounced impact, providing a science-based foundation for sustainable groundwater management and strategic water resource planning. All datasets, versions, spatial/temporal resolutions, pre-processing steps and direct access links are listed in Supplementary Table 1.

Delineation of irrigation regions

We mapped global irrigated regions by identifying contiguous areas with irrigation infrastructure using the 2015 Global Area Equipped for Irrigation dataset[50]. Specifically, we selected pixels where ≥5% of the grid-cell area is classified as area equipped for irrigation in 2015, to delineate coherent irrigation clusters while filtering sparsely irrigated or highly mixed pixels that are less representative of irrigation hotspots and contribute little to region-scale irrigation consumption[51]. Pixel clusters were generated using the Region Group tool in a geographic information system (GIS) environment, applying 'eight-way' connectivity to capture both orthogonal and diagonal spatial relationships among irrigated pixels, as done in the study by Citrini et al.[52]. These preliminary clusters were subsequently refined by spatially overlaying them with HydroBASINS level-6 watershed polygons[53] and subdividing any cluster that crossed watershed boundaries, ensuring that each irrigated region maintains hydrological coherence across upstream and downstream flow paths. This operation treats 'level-6' watershed boundaries as topography-derived cut lines to align region edges with drainage divides; however, the within-region hydrological heterogeneity remains to be addressed in subsequent finer-scale assessments. The resulting irrigated region dataset delineates areas where irrigation water management is a dominant land use, and hydrologic interactions are internally consistent, encompassing many of the world's critical agricultural production zones, including the Indo-Gangetic plains, the California Central Valley, the Yellow River and the Nile Delta.

GWS depletion

We quantified GWS anomalies using the monthly data from the GRACE satellites. Following the approach of Rateb et al.[54], GWS was calculated as follows:

$$\mathrm{GWS} = \mathrm{TWS} - \mathrm{SWS} - \mathrm{SnWS} - \mathrm{SMS}, \tag{1}$$

where the TWS anomaly was obtained as the average of two independent GRACE mascon solutions produced by the Center for Space Research[55] and Jet Propulsion Laboratory[56] processing centres. To isolate GWS, we removed contributions of snow water storage (SnWS) and soil moisture storage (SMS) anomalies based on two models (Noah and VIC) from Global Land Data Assimilation System (GLDAS) reanalysis datasets[57,58]. The surface water storage (SWS) anomaly was derived from a global extension of Zhao et al.[59], which applies the same object-based and scalable remote-sensing method beyond drylands and provides monthly storage-change estimates for individual lakes, reservoirs and wetlands worldwide for 1985–2021. This object-based procedure integrates multi-mission satellite remote sensing (including surface water extent from Landsat and elevation from satellite altimetry) to construct a consistent time series of volumetric changes of SWS. Leveraging this capability, 132,953 waterbodies located within irrigated regions from the HydroLAKES dataset[60] were selected and the SWS time series for each of them were calculated. This approach represents a major advancement in the global monitoring of inland water resources.

The analysis covered the period from April 2002 to December 2021, being limited by the availability of the SWS dataset. All datasets were harmonized at a standard 30 arc-min spatial resolution (~50 km at the Equator) to enable consistent integration. We applied seasonal-trend decomposition using Loess[61] to separate seasonal variability from long-term groundwater trends. Long-term GWS trends were then derived using the Theil–Sen estimator[62,63], a non-parametric statistical method that provides robust trend estimates that are less sensitive to seasonal and interannual fluctuations. Multiplying the annual trends by the number of years studied and normalizing the volume on the actual irrigated areas within each irrigation region allowed us to produce consistent data across two decades of groundwater depletion estimates. Reported uncertainties reflect the semi-amplitude of the two-sided 95% confidence interval of the Theil–Sen trend estimated from the deseasonalized GWS time series and propagated to cumulative changes over 2002–2021.

Surface water availability and HMF estimation

Surface water availability for MAR was assessed using daily river discharge data from the Global Flood Awareness System (GloFAS), version 4.0, developed by the Copernicus Emergency Management Service[64]. GloFAS provides global-scale, observation-driven hydrological estimates generated through the LISFLOOD hydrological model[65], which is forced with the ERA5 atmospheric reanalysis[66]. Lakes and reservoirs are represented in this configuration through a regulation module that attenuates and re-times discharge[67]; in our global analysis we rely on that representation and apply no additional reservoir-specific adjustments. To determine the volumes of surplus surface water available for recharge, we identified HMF events, defined as days when discharge exceeded the 90th and 95th percentile thresholds (representing a less conservative versus more conservative definition of above-threshold capture, respectively) after meeting environmental-flow requirements. Environmental-flow requirements were quantified using the variable monthly flow method[68], which reserves 60%, 45% and 30% of natural monthly flow for the environment during low (<40%), intermediate (40–80%) and high (>80%) flow months, respectively. We computed monthly means and the mean annual flow at each irrigation-region outlet (2002–2021; Supplementary Fig. 7), assigned variable flow fractions month by month, linearly interpolated the monthly environmental-flow requirements to a daily series and subtracted this requirement from daily GloFAS discharge to obtain the available-flow series. The 90th/95th percentiles were then calculated on the daily available discharge record, and the excess above these thresholds was accumulated by month to produce the monthly HMF volumes. These volumes screened by the environmental-flow requirements ensure that MAR interventions do not compromise aquatic ecosystems. This assumption is reasonable for the purpose of our first-cut global screening; however, better estimates of surface-water harvesting volumes will ultimately depend on site-specific legal, institutional and policy constraints. Irrigation-region outlets were identified by intersecting each region's boundary with the GloFAS river network and selecting, among the egressing river cells, the main-stem cell with the highest long-term mean discharge (within a one–two cell neighbourhood to mitigate coastline/boundary artefacts). For regions draining through multiple independent rivers, we defined one outlet per river. Deltaic systems were represented by a single outlet on the distributary with the largest mean discharge. Endorheic regions used the interior cell with the highest long-term discharge (or the terminal waterbody). We used ranking by long-term discharge rather than a fixed absolute threshold because magnitudes vary widely across regions (Supplementary Fig. 7). The concept of utilizing floodwaters and high flows for groundwater recharge has been well-established in regional studies[20,21,23,24,26,69], particularly through strategies such as Agricultural-MAR and Flood-MAR[70,71]. Agricultural-MAR and Flood-MAR involve spreading excess surface water onto agricultural lands or managed basins to enhance infiltration into underlying aquifers, leveraging existing farmland infrastructure to facilitate recharge[69,71]. These methods have been demonstrated as cost-effective and scalable solutions for enhancing water resilience in arid and semi-arid regions, particularly in heavily irrigated agricultural basins. Our analysis extends this framework globally by screening hydrologic opportunities, identifying months and irrigation regions where HMFs coincide with available aquifer space and favourable operational windows for water-spreading MAR. Cumulative HMF volumes were aggregated at the irrigation region scale considering the main outlets within each of them over the April 2002 to December 2021 period, providing a temporally resolved estimate of water surplus potentially available for recharge without undermining environmental-flow requirements (Extended Data Fig. 3).

Region-specific feasibility for HMF capture

HMFs offer windows to divert floodwater for MAR, but the fraction that can actually be infiltrated varies strongly by place and month due to (1) subsurface capacity to accept water, largely governed by permeability and texture[72,73]; (2) concurrent evaporative use during spreading, which is minimized in cool/dormant seasons[74,75]; (3) the share of irrigated land that is off-season and practically available for spreading[76,77]; and (4) cold-season suppression of infiltration in frozen or partially frozen soils[78,79]. Infiltration capacity is also influenced by the hydraulic gradient and water-table depth[80], but these controls are highly site- and time-specific and are not resolved in our global screening; they should therefore be evaluated in subsequent local assessments and design. In addition, many mid-latitude regions experience winter HMF pulses tied to atmospheric rivers, sharpening the seasonal opportunity window[81]. To reflect these controls, we apply a multiplicative feasibility factor $M(r,t) \in [0,1]$ at region r and month t to HMF-derived volumes before the infiltration step (Extended Data Fig. 1a).

$$M(r,t) = \min\{1,\ R(r,t) \times C_{\mathrm{crop}}(r,t)\}, \tag{2}$$

$$R(r,t) = [C_{\mathrm{inf}}(r)]^{w_{\mathrm{inf}}}[1 - C_{\mathrm{ET}}(r,t)]^{w_{\mathrm{ET}}}\,[C_{\mathrm{frost}}(r,t)], \tag{3}$$

with $w_{\mathrm{inf}} + w_{\mathrm{ET}} = 1 w_{\mathrm{inf}} + w_{\mathrm{ET}} = 1$ (we use $w_{\mathrm{inf}} = 0.6$ and $w_{\mathrm{ET}} = 0.4$). All coefficients are dimensionless in $[0,1]$ and defined as C_{inf} infiltration sustainability, C_{ET} evaporative competition, C_{frost} cold-season suppression and C_{crop} crop surface availability. This structure separates rate controls (R: C_{inf}, C_{ET} and C_{frost}) from crop-area availability (C_{crop}), ensures feasibility collapses towards zero when land is fully occupied, and avoids imposing any artificial minimum on the rate itself.

We derived the C_{inf} infiltration suitability coefficient from the GLHYMPS 2.0 global permeability map[73] (Extended Data Fig. 1b). GLHYMPS provides intrinsic permeability as $\log_{10}k$ (square metres). For each irrigation region, we intersected GLHYMPS with a 5 arc-min sampling grid and took the median $\log_{10}k$ across points falling inside each region. The median is preferred to the mean because permeability is highly skewed and spatially heterogeneous; it down-weights small patches of exceptionally coarse or fine materials while better representing near-surface hydrogeologic conditions that control infiltration during spreading. To obtain a dimensionless coefficient $[0,1]$, we

https://doi.org/10.1038/s44221-026-00672-3

mapped the region medians in log-space to a unit interval using a smooth logistic normalization anchored to physically motivated end-members. Specifically, values near $\log_{10}k = -15$ (hydraulic conductivity K, $\sim 10^{-8}$ m s^{-1}, silty/clayey alluvium) are mapped to 0.05, values near $\log_{10}k = -10$ (K, $\sim 10^{-3}$ m s^{-1}, coarse sand–gravel) to 0.95 and the mid-range, −12.5, mapping near 0.50 (ref. 82). This soft-bounded transform avoids hard truncation and literal 0/1 while preserving the intended ordering-regions underlain by coarser, better-drained materials receive higher infiltration suitability (Extended Data Fig. 1b).

We derived the monthly C_{ET} evapotranspiration (ET) coefficient for each irrigated region to represent how much ET would oppose infiltration during spreading (Extended Data Fig. 1c). First, we extracted monthly ET from two independent land-surface models (GLDAS-Noah and VIC) on a common grid and aggregated to irrigation regions (median across grid points). Because ET varies both absolutely across climates and seasonally within a region, we used a two-step normalization to obtain a dimensionless feasibility factor in $[0, 1]$, where higher values indicate lower evaporative competition (that is, more favourable months for spreading). In a global energy context, we ranked all region–month ET values together and mapped them monotonically so that climatologically low ET (cool, low-radiation months typical of winter) receives values near 1, and high ET (hot, high-radiation months) near 0. This step avoids penalizing cool regions simply because they are energy-limited overall. In a region-relative seasonality context, within each region, we summarized its multi-year monthly cycle (from January to December) and rescaled those 12 climatological values to highlight the local off-season window (winter months score high, summer months low). Finally, we combined the global and region-relative signatures into a single monthly coefficient and gently kept all values within $[0, 1]$ to avoid pathological zeros or ones. The result is a conservative ET penalty that is high in cool months and low in hot months, aligned with operational practice for spreading (Extended Data Fig. 1c).

To reflect the suppression of infiltration under frozen or partially frozen soils, we derived a monthly C_{frost} coefficient for each irrigation region from 2-m air temperature. We first extracted monthly air temperature from GLDAS for two independent land-surface models (GLDAS-Noah and VIC) on a common grid, aggregated each to irrigation regions by taking the median across grid points and then formed a single series per region-month as the cross-model median. We then mapped region-month temperatures to a three-level frost coefficient that penalizes months when frozen soils are likely to limit intake: $T > 2$ °C equals 1.0 (no frost penalty; soils expected to be unfrozen or fully thawed), $0 < T \leq 2$ °C equals 0.5 (partial thaw; reduced but not negligible intake) and $T \leq 0$ °C equals 0.1 (frozen conditions; strong reduction in intake). These thresholds encode widely documented behaviour: the hydraulic conductivity and infiltrability of soils drop sharply as liquid water is replaced by ice near and below 0 °C; partial thaw conditions can permit some focused or preferential infiltration, but system-level intake is still curtailed[78]. The scheme is intentionally simple and conservative for global application, while aligned with cold-region hydrology literature and modelling of frozen-soil infiltration.

We quantified, for each irrigation region and month, the fraction of surface area that is realistically available for spreading given ongoing crop occupancy (C_{crop}) (Extended Data Fig. 1d). We used MIRCA-OS monthly growing-area grids (5 arc-min) for years 2000, 2005, 2010 and 2015[83], and aggregated them to irrigation regions (area-weighted sum). MIRCA-OS provides separate crop calendars and associated growing/harvested areas for irrigated and rainfed systems; here, we use only the irrigated layers, which report harvested/growing area (ha) by month, to characterize seasonal land occupancy within the irrigated agricultural footprint. Rainfed cropping can also constrain land availability locally, but it is not explicitly represented in C_{crop} in this first-order global screening and should be addressed in subsequent basin- and site-scale assessments. For each month, we summed the irrigated area of 17 major crops: wheat, maize, rice, barley, millet, sorghum, soybean, sunflower, potato, cassava, sugarcane, sugar beet, oil palm, rapeseed/canola, groundnut/peanut, rye and cotton. We then expressed monthly crop occupancy as the ratio of this summed area to the region's peak monthly irrigated area (the maximum monthly total over the year, used as the region-level irrigated footprint). To avoid double counting where multiple crops might co-occur within pixels, the monthly sum was capped by that peak footprint. We use a conservative 10% lower bound to represent incidental infiltration pathways that persist even when mapped occupancy approaches 100%, notably unlined conveyance canals and laterals, drains and sumps, farm roads and margins, and temporarily idle patches, which routinely admit water outside planted rows. Seepage from earthen/unlined canals is widely documented at multi-percent to tens-of-percent of flow, with typical values ~10–20% and higher in some systems[84,85] (Extended Data Fig. 1d).

Unsustainable irrigation water consumption

Monthly unsustainable irrigation was quantified at a 30 arc-min resolution (50 km at the Equator) using a water-balance approach, building on the framework developed by previous studies[5,52,86–89]. Unsustainable irrigation water consumption was calculated over the 2002–2021 period as the portion of irrigation water consumption that exceeded locally renewable water availability. Renewable water availability was determined as local surface and subsurface blue-water availability remaining after accounting for environmental flows[68] and other human water consumptions. To enforce mass conservation and upstream–downstream consistency, we then route this residual renewable blue water downstream using eight-direction flow routing, so that upstream contributions are accumulated before entering downstream cells and are not double counted. As a result, this unsustainable irrigation analysis is source-agnostic: it quantifies the portion of irrigation consumptive use that exceeds contemporaneous renewable blue-water inflow, independent of the prevailing split between surface- and groundwater consumptions. Blue-water inputs and irrigation water consumption (Supplementary Fig. 8) were sourced from the Inter-Sectoral Impact Model Intercomparison Project ISIMIP3b ensemble[90] (H08[91,92] and WaterGAP2-2e[93] hydrological models) forced by five Coupled Model Intercomparison Project (CMIP6) global climate models under historical climate forcing and fixed 2015 socioeconomic conditions (GFDL-ESM4, IPSL-CM6A-LR, MPI-ESM1-2HR, MRI-ESM2-0 and UKESM1-0-LL). The other inter-sectoral water consumptions (for example, domestic, manufacturing, mining, electric generation and livestock) were isolated and kept constant from multi-sectoral water-use estimates derived from Huang et al.[94] on the basis of the 2001–2010 data.

In addition, we contextualized the unsustainable irrigation water consumption by cross-referencing a widely used map of groundwater-sourced irrigation (Global Map of Irrigation Areas version 5)[95]. To place the datasets on a common resolution, we aggregated that dataset to the irrigation-region scale using area-weighted means and reported regional values in four classes (0–25%, 25–50%, 50–75% and 75–100%) (Supplementary Fig. 6).

Assessment of the effect of MAR-scenario deployment

To quantify the potential impact of MAR on alleviating unsustainable irrigation, we developed a dynamic simulation framework that contrasts historical irrigation deficits with a MAR-scenario in which surplus surface water is diverted for recharge. The analysis covers the 2002–2021 period and is performed using a monthly time-step.

The dynamic simulation framework was implemented to simulate monthly infiltration and groundwater extraction. The MAR-scenario is formulated as a monthly regional mass balance in which EFR-screened HMF volumes are first pre-scaled by the region- and monthly-specific feasibility coefficient M, recharge is limited by the GRACE-derived recoverable storage cap and subsequent extraction offsets modelled unsustainable irrigation subject to available stored volume. Recoverable storage was defined as the cumulative GRACE-derived groundwater depletion over 2002–2021, providing a consistent restoration target across irrigation regions. This volumetric threshold represents recoverable storage that can feasibly be replenished through MAR, beyond which additional recharge is assumed to be physically or operationally constrained. We define each region's available storage cap as the cumulative GRACE-inferred groundwater loss over 2002–2021. In the monthly accounting we track the remaining recoverable aquifer capacity, computed as the fixed cap minus the MAR volume in storage at the end of each month. For each irrigated region and month, the infiltrated volume was computed as the minimum between HMF and the aquifer's available storage capacity. This volume was then included in the dynamic monthly assessment of GWS. To offset unsustainable irrigation, we allow monthly extraction up to the available stock, defined as the stored volume after accounting for that month's feasibility-weighted infiltration and subject to the GRACE-derived storage cap, so extraction may draw on both carryover storage and recharge in the current month but never exceeds the available stock. The model updated both GWS and remaining capacity at each time-step. Simulations were executed separately for both the 90th and 95th percentile HMF scenarios. These results provided the basis for comparing observed irrigation stress with MAR-scenario outcomes, allowing us to quantify the maximum feasible contribution of MAR to global agricultural water sustainability in terms of percentage. We exclude irrigation regions from the MAR-offset calculation when (1) the unsustainable irrigation water consumption assessment reports zero over the analysis period (that is, irrigation consumptive use does not exceed contemporaneous renewable blue-water inflow after environmental-flow reservations and routing) and/or (2) the recoverable storage cap is zero, which we take to occur when the cumulative GRACE-inferred GWS change over 2002–2021 is non-positive within the irrigated-region polygon. This exclusion does not speak to implementability, it simply denotes regions where, under our definitions, there is no irrigation deficit to reduce and/or no recoverable aquifer capacity to bank additional recharge. Finally, to represent variability in infrastructure and operational performance, we report both the feasibility-weighted case and a set of uniform capture-efficiency benchmarks. In the benchmark runs, 100%, 50% and 10% capture efficiencies were applied multiplicatively to HMF volumes before the infiltration step of the MAR-scenario analysis, providing a consistent basis for comparison under both HMF percentile thresholds. The framework does not explicitly simulate reservoir operations, conveyance constraints, water-quality treatment or site-scale hydrogeologic heterogeneity; these factors are therefore represented only indirectly through M and the benchmark capture-efficiency scenarios.

Analysis for dominant limitation and irrigation consumption pressure

To interpret spatial patterns in MAR offset potential and to identify the dominant limiting factor across irrigation regions, we derived two complementary, period-integrated diagnostics from the same volumes used in the MAR-scenario simulations. For each irrigated region, we first computed the cumulative feasibility-weighted high-magnitude-flow supply (S_p),

$$S_p = \sum_t \mathrm{HMF}_{p,t}, \tag{4}$$

where p denotes the percentile threshold scenario (90th and 95th percentiles) and $\mathrm{HMF}_{p,t}$ is the monthly EFR-screened feasibility-weighted HMF volume (cubic kilometres) used for the infiltration phase. We also defined the recoverable storage cap (C) as the cumulative groundwater loss over the 2002–2021 period (the maximum aquifer storage capacity, as above, in cubic kilometres) and the cumulative unsustainable irrigation water consumption (UIWC, in cubic kilometres) over the same period. We then calculated a constraint ratio (CR) for each HMF scenario, which diagnoses whether MAR opportunities are primarily limited by the availability of above-threshold surface-water supply or by the selected restoration target (the recoverable storage cap).

$$\mathrm{CR}_p = \frac{S_p}{C}. \tag{5}$$

Regions with CR_p <1 are classified as HMF-supply constrained (cumulative feasible HMF supply is insufficient to fill the recoverable storage cap), whereas regions with CR_p ≥1 are classified as depletion-cap constrained (feasible HMF supply exceeds the recoverable cap, such that the cap becomes the binding constraint in the period-integrated balance).

To quantify how strongly unsustainable irrigation demand exceeds the maximum recharge volume that can be banked under the MAR-scenario assumptions, we also computed an Irrigation Consumption Pressure Index (ICPI),

$$\mathrm{ICPI}_p = \frac{\mathrm{UIWC}}{\min(S_p, C)}. \tag{6}$$

This index quantifies the relative magnitude of cumulative unsustainable irrigation consumption compared with the maximum feasible banked recharge volume over 2002–2021. Values of ICPI_p >1 indicate that cumulative unsustainable irrigation consumption exceeds the period-integrated recharge capacity (partial offset), whereas ICPI_p ≤1 indicates that the cumulative feasible recharge capacity is sufficient to fully offset unsustainable irrigation consumption under the scenario assumptions (full-offset potential). Both diagnostics were computed for the 90th and 95th percentile HMF scenarios and are used to support interpretation of the offset maps by separating supply- versus storage-cap constraints and by quantifying irrigation consumption dominance. For mapping, ICPI_p was binned into equivalent upper-bound offset classes using the inverse mapping ($\mathrm{ICPI}_p \geq 20$ corresponds to <5% of feasible offset, $10 \leq \mathrm{ICPI}_p < 20$ corresponds to 5–10% of feasible offset, $5 \leq \mathrm{ICPI}_p < 10$ corresponds to 10–20% of feasible offset, $2 \leq \mathrm{ICPI}_p < 5$ corresponds to 20–50% of feasible offset and $\mathrm{ICPI}_p < 2$ corresponds to 50–100% of feasible offset). Unlike Fig. 3, these classes are derived from cumulative 2002–2021 balances to separate whether low offsets reflect limited recharge capacity relative to consumption, independent of within-year timing and carryover effects captured by the monthly simulation.

Data availability

Data supporting the findings of this study are available within the article and its Supplementary Information. Results are available via Zenodo at https://doi.org/10.5281/zenodo.15731808 (ref. 96).

Code availability

Data analysis was performed using Python 3.11.0, utilizing the following packages: PySheds (0.3.5), Xarray (2022.11.0), Cartopy (0.21.1), GeoPandas (0.12.1), Matplotlib (3.6.2), Pandas (1.5.2) and NumPy (1.23.5). Spatial figure preparation was also carried out in ArcGIS Pro (version 3.3.0, Esri). Custom scripts and functions developed for this study are available from the corresponding author upon reasonable request.

References

1. Rosa, L. Adapting agriculture to climate change via sustainable irrigation: biophysical potentials and feedbacks. *Environ. Res. Lett.* **17**, 063008 (2022).
2. Tack, J., Barkley, A. & Hendricks, N. Irrigation offsets wheat yield reductions from warming temperatures. *Environ. Res. Lett.* **12**, 114027 (2017).
3. Kuang, X. et al. The changing nature of groundwater in the global water cycle. *Science* **383**, eadf0630 (2024).

4. Taylor, R. G. et al. Ground water and climate change. *Nat. Clim. Change* **3**, 322–329 (2013).
5. Rosa, L., Chiarelli, D. D., Tu, C., Rulli, M. C. & D'Odorico, P. Global unsustainable virtual water flows in agricultural trade. *Environ. Res. Lett.* **14**, 114001 (2019).
6. Döll, P., Müller Schmied, H., Schuh, C., Portmann, F. T. & Eicker, A. Global-scale assessment of groundwater depletion and related groundwater abstractions: combining hydrological modeling with information from well observations and GRACE satellites. *Water Resour. Res.* **50**, 5698–5720 (2014).
7. Rodell, M. et al. Emerging trends in global freshwater availability. *Nature* **557**, 651–659 (2018).
8. De Graaf, I. E. M., Gleeson, T., Rens Van Beek, L. P. H., Sutanudjaja, E. H. & Bierkens, M. F. P. Environmental flow limits to global groundwater pumping. *Nature* **574**, 90–94 (2019).
9. Niazi, H. et al. Global peak water limit of future groundwater withdrawals. *Nat. Sustain.* **7**, 413–422 (2024).
10. Davis, K. F., Rulli, M. C., Seveso, A. & D'Odorico, P. Increased food production and reduced water use through optimized crop distribution. *Nat. Geosci.* **10**, 919–924 (2017).
11. Schmitt, R. J. P., Rosa, L. & Daily, G. C. Global expansion of sustainable irrigation limited by water storage. *Proc. Natl Acad. Sci. USA* **119**, e2214291119 (2022).
12. Schmitt, R. J. P. & Rosa, L. Dams for hydropower and irrigation: trends, challenges, and alternatives. *Renew. Sustain. Energy Rev.* **199**, 114439 (2024).
13. Kahn, M., Sangiorgio, M. & Rosa, L. Potential of wastewater reuse to alleviate water scarcity under future warming scenarios. *Environ. Res. Lett.* **20**, 034012 (2025).
14. Van Vliet, M. T. H. et al. Global water scarcity including surface water quality and expansions of clean water technologies. *Environ. Res. Lett.* **16**, 024020 (2021).
15. Rosa, L., Gabrielli, P. & Sangiorgio, M. Global energy, costs, and emissions from reverse osmosis desalination under future water scarcity. *Water Res.* **289**, 124825 (2026).
16. Siddik, M. A. B., Dickson, K. E., Rising, J., Ruddell, B. L. & Marston, L. T. Interbasin water transfers in the United States and Canada. *Sci. Data* **10**, 27 (2023).
17. Mekonnen, M. M. et al. Trends and environmental impacts of virtual water trade. *Nat. Rev. Earth Environ.* **5**, 890–905 (2024).
18. Lord, J. et al. Global potential for harvesting drinking water from air using solar energy. *Nature* **598**, 611–617 (2021).
19. Scanlon, B. R. et al. Global water resources and the role of groundwater in a resilient water future. *Nat. Rev. Earth Environ.* **4**, 87–101 (2023).
20. Dillon, P. et al. Sixty years of global progress in managed aquifer recharge. *Hydrogeol. J.* **27**, 1–30 (2019).
21. Levintal, E. et al. Agricultural managed aquifer recharge (Ag-MAR)—a method for sustainable groundwater management: a review. *Crit. Rev. Environ. Sci. Technol.* **53**, 291–314 (2023).
22. He, X. et al. Climate-informed hydrologic modeling and policy typology to guide managed aquifer recharge. *Sci. Adv.* **7**, eabe6025 (2021).
23. Kocis, T. N. & Dahlke, H. E. Availability of high-magnitude streamflow for groundwater banking in the Central Valley, California. *Environ. Res. Lett.* **12**, 084009 (2017).
24. Kourakos, G., Brunetti, G., Bigelow, D. P., Wallander, S. & Dahlke, H. E. Optimizing managed aquifer recharge locations in California's Central Valley using an evolutionary multi-objective genetic algorithm coupled with a hydrological simulation model. *Water Resour. Res.* **59**, e2022WR034129 (2023).
25. Yang, Q. & Scanlon, B. R. How much water can be captured from flood flows to store in depleted aquifers for mitigating floods and droughts? A case study from Texas, US. *Environ. Res. Lett.* **14**, 054011 (2019).
26. Dillon, P., Fernández Escalante, E., Megdal, S. B. & Massmann, G. Managed aquifer recharge for water resilience. *Water* **12**, 1846 (2020).
27. Rodell, M. & Famiglietti, J. S. The potential for satellite-based monitoring of groundwater storage changes using GRACE: the High Plains aquifer, Central US. *J. Hydrol.* **263**, 245–256 (2002).
28. Famiglietti, J. S. in *Geophysical Monograph Series* Vol. 150 (eds Sparks, R. S. J. & Hawkesworth, C. J.) 197–207 (American Geophysical Union, 2004).
29. Clarke, B., Otto, F., Stuart-Smith, R. & Harrington, L. Extreme weather impacts of climate change: an attribution perspective. *Environ. Res. Clim.* **1**, 012001 (2022).
30. Yuan, J., Van Dyke, M. I. & Huck, P. M. Water reuse through managed aquifer recharge (MAR): assessment of regulations/guidelines and case studies. *Water Qual. Res. J. Can.* **51**, 357–376 (2016).
31. Alam, S., Gebremichael, M., Li, R., Dozier, J. & Lettenmaier, D. P. Can managed aquifer recharge mitigate the groundwater overdraft in California's Central Valley? *Water Resour. Res.* **56**, e2020WR027244 (2020).
32. Ganot, Y. et al. Managed aquifer recharge with reverse-osmosis desalinated seawater: modeling the spreading in groundwater using stable water isotopes. *Hydrol. Earth Syst. Sci.* **22**, 6323–6333 (2018).
33. Goharian, E., Azizipour, M., Sandoval-Soils, S. & Fogg, G. E. Surface reservoir reoperation for managed aquifer recharge: folsom reservoir system. *J. Water Resour. Plan. Manag.* **146**, 04020095 (2020).
34. Speijer, L. et al. Enhancing groundwater recharge in drinking water protection zones in Flanders (Belgium): a novel approach to assess stormwater managed aquifer recharge potential. *J. Hydrol. Reg. Stud.* **53**, 101747 (2024).
35. Alam, M. F. & Pavelic, P. *Underground Transfer of Floods for Irrigation (UTFI): Exploring Potential at the Global Scale* (International Water Management Institute, 2020); https://hdl.handle.net/10568/109588, https://doi.org/10.5337/2020.204
36. Martinsen, G. et al. Large-scale hydrological modeling in a multi-objective uncertainty framework – assessing the potential for managed aquifer recharge in the North China Plain. *J. Hydrol. Reg. Stud.* **41**, 101097 (2022).
37. Brindha, K. & Pavelic, P. Identifying priority watersheds to mitigate flood and drought impacts by novel conjunctive water use management. *Environ. Earth Sci.* **75**, 399 (2016).
38. Carlson, G. et al. Intensive irrigation buffers groundwater declines in key European breadbasket. *Nat. Water* https://doi.org/10.1038/s44221-025-00445-4 (2025).
39. Dangar, S. & Mishra, V. Natural and anthropogenic drivers of the lost groundwater from the Ganga River basin. *Environ. Res. Lett.* **16**, 114009 (2021).
40. Panda, D. K., Ambast, S. K. & Shamsudduha, M. Groundwater depletion in northern India: impacts of the sub-regional anthropogenic land-use, socio-politics and changing climate. *Hydrol. Process.* **35**, e14003 (2021).
41. Scanlon, B. R., Reedy, R. C., Faunt, C. C., Pool, D. & Uhlman, K. Enhancing drought resilience with conjunctive use and managed aquifer recharge in California and Arizona. *Environ. Res. Lett.* **11**, 035013 (2016).
42. Scanlon, B. R., Longuevergne, L. & Long, D. Ground referencing GRACE satellite estimates of groundwater storage changes in the California Central Valley, USA. *Water Resour. Res.* **48**, 2011WR011312 (2012).
43. Liu, P.-W. et al. Groundwater depletion in California's Central Valley accelerates during megadrought. *Nat. Commun.* **13**, 7825 (2022).
44. Farkas, J. Z., Hoyk, E. & Rakonczai, J. Geographical analysis of climate vulnerability at a regional scale: the case of the Southern Great Plain in Hungary. *Hung. Geogr. Bull.* **66**, 129–144 (2017).

45. Zheng, Y., Vanderzalm, J., Hartog, N., Escalante, E. F. & Stefan, C. The 21st century water quality challenges for managed aquifer recharge: towards a risk-based regulatory approach. *Hydrogeol. J.* **31**, 31–34 (2023).
46. Ross, A. & Hasnain, S. Factors affecting the cost of managed aquifer recharge (MAR) schemes. *Sustain. Water Resour. Manag.* **4**, 179–190 (2018).
47. Dillon, P. J., Alley, W., Zheng, Y. & Vanderzalm, J. *Managed Aquifer Recharge: Overview and Governance* (International Association of Hydrogeologists, 2022).
48. Natural Resource Management Ministerial Council, Environment Protection and Heritage Council, and National Health and Medical Research Council. *Australian Guidelines for Water Recycling: Managing Health and Environmental Risks (Phase 2). Managed Aquifer Recharge*. 252 https://www.waterquality.gov.au/sites/default/files/documents/water-recycling-guidelines-mar-24.pdf (2009).
49. Jasechko, S. Global cases of groundwater recovery after interventions. *Science* **391**, 1218–1228 (2026).
50. Mehta, P. et al. Half of twenty-first century global irrigation expansion has been in water-stressed regions. *Nat. Water* **2**, 254–261 (2024).
51. Puy, A., Borgonovo, E., Lo Piano, S., Levin, S. A. & Saltelli, A. Irrigated areas drive irrigation water withdrawals. *Nat. Commun.* **12**, 4525 (2021).
52. Citrini, A., Sangiorgio, M. & Rosa, L. Global multi-model trends of unsustainable irrigation under climate change scenarios. *Environ. Res. Lett.* **20**, 104011 (2025).
53. Lehner, B. & Grill, G. Global river hydrography and network routing: baseline data and new approaches to study the world's large river systems. *Hydrol. Process.* **27**, 2171–2186 (2013).
54. Rateb, A. et al. Comparison of groundwater storage changes from GRACE satellites with monitoring and modeling of major U.S. aquifers. *Water Resour. Res.* **56**, e2020WR027556 (2020).
55. Save, H., Bettadpur, S. & Tapley, B. D. High-resolution CSR GRACE RL05 mascons. *J. Geophys. Res. Solid Earth* **121**, 7547–7569 (2016).
56. Watkins, M. M., Wiese, D. N., Yuan, D., Boening, C. & Landerer, F. W. Improved methods for observing Earth's time variable mass distribution with GRACE using spherical cap mascons. *J. Geophys. Res. Solid Earth* **120**, 2648–2671 (2015).
57. Rodell, M. et al. The global land data assimilation system. *Bull. Am. Meteorol. Soc.* **85**, 381–394 (2004).
58. Beaudoing, H. GLDAS VIC Land Surface Model L4 monthly 1.0 x 1.0 degree V2.1. *NASA Goddard Earth Sciences Data and Information Services Center* https://doi.org/10.5067/VWTH7S6218SG (2020).
59. Zhao, G. et al. Decoupling of surface water storage from precipitation in global drylands due to anthropogenic activity. *Nat. Water* **3**, 80–88 (2025).
60. Messager, M. L., Lehner, B., Grill, G., Nedeva, I. & Schmitt, O. Estimating the volume and age of water stored in global lakes using a geo-statistical approach. *Nat. Commun.* **7**, 13603 (2016).
61. Cleveland, R. B., Cleveland, W. S., McRae, J. E. & Terpenning, I. STL: a seasonal-trend decomposition procedure based on Loess. *J. Off. Stat.* **6**, 3–37 (1990).
62. Sen, P. K. Estimates of the regression coefficient based on Kendall's Tau. *J. Am. Stat. Assoc.* **63**, 1379–1389 (1968).
63. Theil, S. A rank-invariant method of linear and polynomial regression analysis. *Indag. Math.* **12**, 173 (1950).
64. Zsoter, E. River discharge historical data from the Global Flood Awareness System. *Climate Data Store* https://doi.org/10.24381/cds.a4fdd6b9 (2019).
65. Van Der Knijff, J. M., Younis, J. & De Roo, A. P. J. LISFLOOD: a GIS-based distributed model for river basin scale water balance and flood simulation. *Int. J. Geogr. Inf. Sci.* **24**, 189–212 (2010).
66. Hersbach, H. et al. The ERA5 global reanalysis. *Q. J. R. Meteorol. Soc.* **146**, 1999–2049 (2020).
67. Harrigan, S. et al. GloFAS-ERA5 operational global river discharge reanalysis 1979–present. *Earth Syst. Sci. Data* **12**, 2043–2060 (2020).
68. Pastor, A. V., Ludwig, F., Biemans, H., Hoff, H. & Kabat, P. Accounting for environmental flow requirements in global water assessments. *Hydrol. Earth Syst. Sci.* **18**, 5041–5059 (2014).
69. Dahlke, H. E. et al. in *Advances in Chemical Pollution, Environmental Management and Protection* Vol. 3 (eds Friesen, J. & Rodríguez-Sinobas, L.) Ch. 8 (Elsevier, 2018).
70. Marr, J., Arrate, D., Maendly, R., Dhillon, D. & Stygar, S. *Flood-MAR: Using Flood Water for Managed Aquifer Recharge to Support Sustainable Water Resources* (California Department of Water Resources, 2018).
71. Niswonger, R. G., Morway, E. D., Triana, E. & Huntington, J. L. Managed aquifer recharge through off-season irrigation in agricultural regions. *Water Resour. Res.* **53**, 6970–6992 (2017).
72. Alam, S., Borthakur, A., Ravi, S., Gebremichael, M. & Mohanty, S. K. Managed aquifer recharge implementation criteria to achieve water sustainability. *Sci. Total Environ.* **768**, 144992 (2021).
73. Huscroft, J., Gleeson, T., Hartmann, J. & Börker, J. Compiling and mapping global permeability of the unconsolidated and consolidated Earth: GLobal HYdrogeology MaPS 2.0 (GLHYMPS 2.0). *Geophys. Res. Lett.* **45**, 1897–1904 (2018).
74. Ulibarri, N., Escobedo Garcia, N., Nelson, R. L., Cravens, A. E. & McCarty, R. J. Assessing the feasibility of managed aquifer recharge in California. *Water Resour. Res.* **57**, e2020WR029292 (2021).
75. Dahlke, H. E., Brown, A. G., Orloff, S., Putnam, D. & O'Geen, T. Managed winter flooding of alfalfa recharges groundwater with minimal crop damage. *Calif. Agric.* **72**, 1–11 (2018).
76. Portmann, F. T., Siebert, S. & Döll, P. MIRCA2000—Global monthly irrigated and rainfed crop areas around the year 2000: a new high-resolution data set for agricultural and hydrological modeling. *Glob. Biogeochem. Cycles* **24**, 2008GB003435 (2010).
77. Laborte, A. G. et al. RiceAtlas, a spatial database of global rice calendars and production. *Sci. Data* **4**, 170074 (2017).
78. Kurylyk, B. L. & Watanabe, K. The mathematical representation of freezing and thawing processes in variably-saturated, non-deformable soils. *Adv. Water Resour.* **60**, 160–177 (2013).
79. Heinze, T. A multi-phase heat transfer model for water infiltration into frozen soil. *Water Resour. Res.* **57**, e2021WR030067 (2021).
80. Bouwer, H. Artificial recharge of groundwater: hydrogeology and engineering. *Hydrogeol. J.* **10**, 121–142 (2002).
81. Zhou, Y. et al. Characteristics and variability of winter northern Pacific atmospheric river flavors. *J. Geophys. Res. Atmos.* **127**, e2022JD037105 (2022).
82. Freeze, R. A. & Cherry, J. A. *Groundwater* (Prentice-Hall, 1979).
83. Kebede, E. et al. A global open-source dataset of monthly irrigated and rainfed cropped areas (MIRCA-OS) for the 21st century. *HydroShare* https://doi.org/10.4211/hs.60a890eb841c460192c03bb590687145 (2024).
84. Gad, M., Abdelhaleem, H. M. & Waleed, O. A. S. Forecasting the seepage loss for lined and un-lined canals using artificial neural network and gene expression programming. *Geomat. Nat. Hazards Risk* **14**, 2221775 (2023).
85. Barkhordari, S. & Hashemy Shahdany, S. M. A systematic approach for estimating water losses in irrigation canals. *Water Sci. Eng.* **15**, 161–169 (2022).
86. Rosa, L. et al. Potential for sustainable irrigation expansion in a 3 °C warmer climate. *Proc. Natl Acad. Sci. USA* **117**, 29526–29534 (2020).
87. Rosa, L. & He, L. Global multi-model projections of green water scarcity risks in rainfed agriculture under 1.5 °C and 3 °C warming. *Agric. Water Manage.* **314**, 109519 (2025).
88. Rosa, L. et al. Closing the yield gap while ensuring water sustainability. *Environ. Res. Lett.* **13**, 104002 (2018).

89. Rosa, L. & Sangiorgio, M. Global water gaps under future warming levels. *Nat. Commun.* **16**, 1192 (2025).
90. Gosling, S. N. et al. ISIMIP3a simulation data from the global water sector. *ISIMIP Repository* https://doi.org/10.48364/ISIMIP.398165.2 (2024).
91. Hanasaki, N., Yoshikawa, S., Pokhrel, Y. & Kanae, S. A global hydrological simulation to specify the sources of water used by humans. *Hydrol. Earth Syst. Sci.* **22**, 789–817 (2018).
92. Yoshida, T. et al. Inference of parameters for a global hydrological model: identifiability and predictive uncertainties of climate-based parameters. *Water Resour. Res.* **58**, e2021WR030660 (2022).
93. Müller Schmied, H. et al. The global water resources and use model WaterGAP v2.2e: description and evaluation of modifications and new features. *Geosci. Model Dev.* **17**, 8817–8852 (2024).
94. Huang, Z. et al. Reconstruction of global gridded monthly sectoral water withdrawals for 1971–2010 and analysis of their spatiotemporal patterns. *Hydrol. Earth Syst. Sci.* **22**, 2117–2133 (2018).
95. Siebert, S., Henrich, V., Frenken, K. & Burke, J. *Update of the Digital Global Map of Irrigation Areas to Version 5* Vol. 10, 2660–6728 (Rheinische Friedrich-Wilhelms-Universität and Food and Agriculture Organization of the United Nations, 2013).
96. Citrini, A. et al. Supplementary Information for "Global managed aquifer recharge potential as a solution to water scarcity". *Zenodo* https://doi.org/10.5281/zenodo.15731808 (2026).

Author contributions
A.C. and L.R. conceived the study. A.C. led the analysis and wrote the paper. A.C., B.R.S. and L.R. designed the research with input from all authors. A.R. contributed key datasets and provided technical support for groundwater depletion assessment. G.Z. developed and processed essential geospatial datasets for surface water storage. M.S. contributed analytical tools and supported the development of the modelling framework for unsustainable irrigation. L.R. supervised the research activities and supported interpretation of results. All authors contributed to discussions and reviewed the final paper.

Funding
L.R. discloses support of this work from Schmidt Sciences, LLC.

Competing interests
The authors declare no competing interests.

Additional information
Extended data is available for this paper at https://doi.org/10.1038/s44221-026-00672-3.

Supplementary information The online version contains supplementary material available at https://doi.org/10.1038/s44221-026-00672-3.

Correspondence and requests for materials should be addressed to Lorenzo Rosa.

Peer review information *Nature Water* thanks Mohammad Faiz Alam, Matthew Rodell and Joanne Vanderzalm for their contributions to the peer review of this work. Peer reviewer reports are available.

https://doi.org/10.1038/s44221-026-00672-3

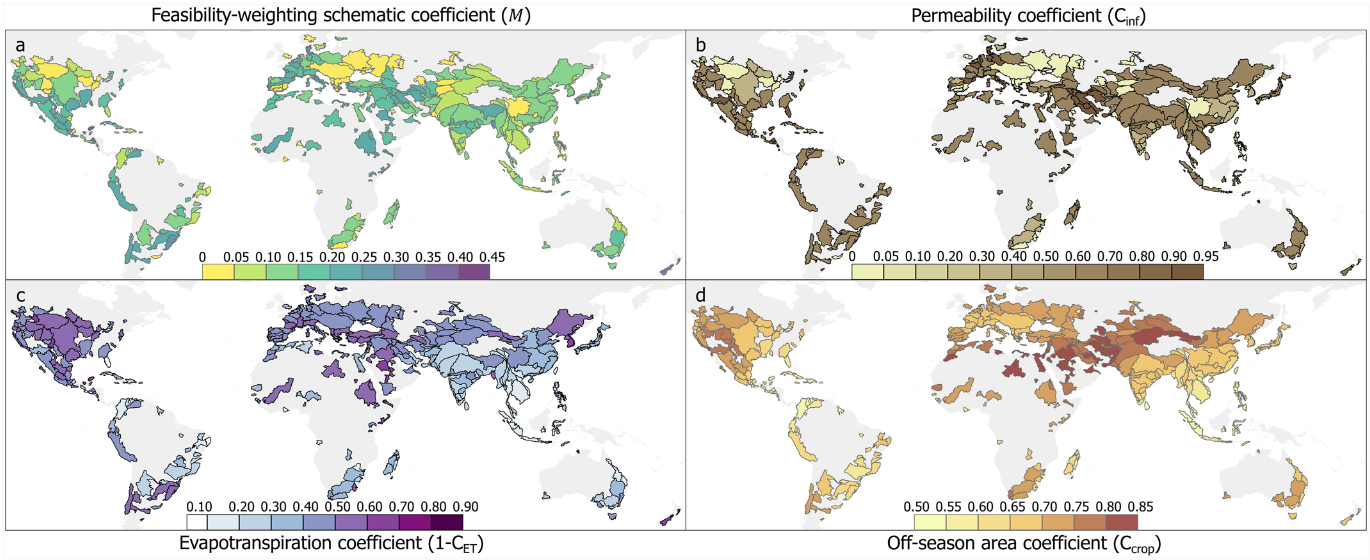

Extended Data Fig. 1 | Basin-specific feasibility factors used in the MAR-scenario analysis. Maps are shown at the irrigation-region scale. **a**, Multi-year median of the monthly feasibility coefficient $M(r,t) \in [0,1]$. **b**, Infiltration-suitability coefficient $C\,\inf(r) \in [0,1]$. **c**, Evapotranspiration coefficient $1 - C_{ET}(r,t) \in [0,1]$, for which higher values indicate lower evapotranspiration competition and thus more favorable months for MAR. **d**, Off-season crop-area availability $Ccrop(r,t) \in [0,1]$. All coefficients are dimensionless; warmer colors generally denote greater feasibility, except in panel **c**, where the scale reflects lower evapotranspiration competition. Basemap data from Esri, Garmin International, Inc., the US Central Intelligence Agency (The World Factbook) and the National Geographic Society.

 https://doi.org/10.1038/s44221-026-00672-3

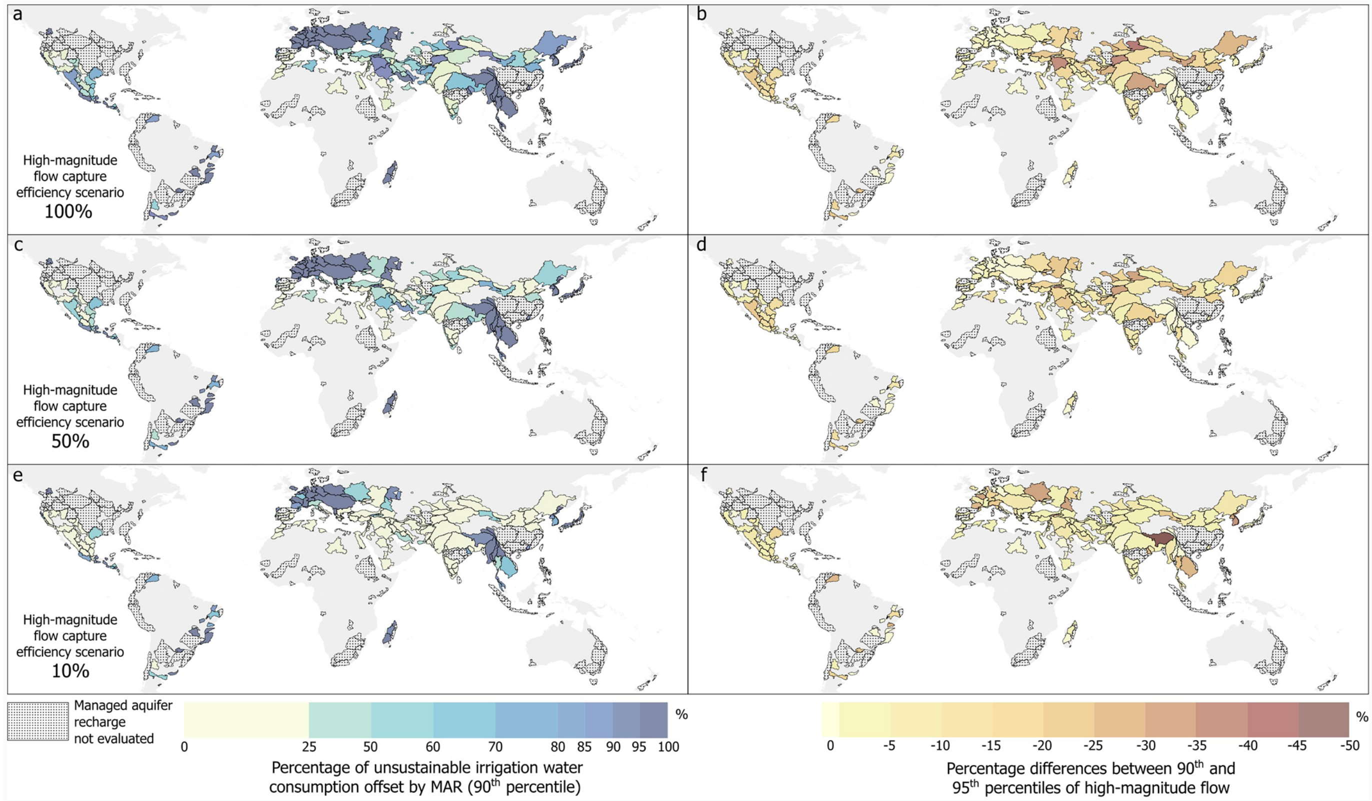

Extended Data Fig. 2 | Sensitivity of MAR offset potential to HMF capture-efficiency and threshold assumptions. Percentage of unsustainable irrigation water consumption offset by MAR under three HMF capture-efficiency scenarios—100% (**a**,**b**), 50% (**c**,**d**) and 10% (**e**,**f**)—for the 90th-percentile HMF threshold (left column) and the percentage difference between the 90th and 95th percentile scenarios (right column). These scenarios represent varying assumptions about infrastructure and institutional capacity to capture and store high-magnitude flows. Grey hatching indicates areas where MAR was not evaluated because modeled unsustainable irrigation water consumption was zero and/or groundwater depletion was not detected. Basemap data from Esri, Garmin International, Inc., the US Central Intelligence Agency (The World Factbook) and the National Geographic Society.

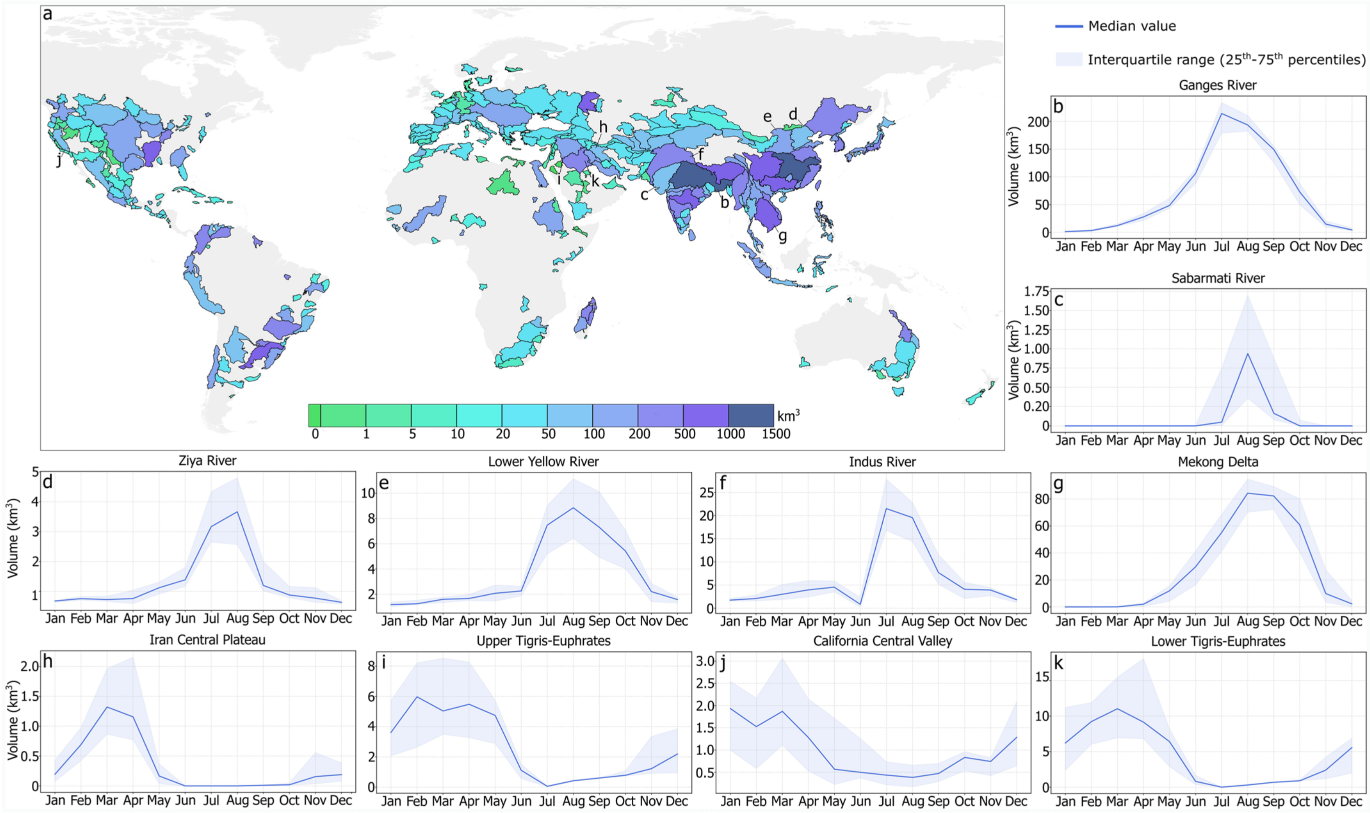

Extended Data Fig. 3 | Accumulated high-magnitude flow and seasonal discharge variability in representative irrigation regions. a, Global distribution of accumulated high-magnitude flow volume (cubic kilometres) from 2002 to 2021, based on the 90th-percentile threshold of daily discharge derived from GloFAS[67]. Darker blue-to-purple colors indicate higher cumulative HMF volumes. **b**–**k**, monthly discharge patterns in a selection of major irrigation regions heavily impacted by groundwater depletion, showing the median and interquartile range (25th-75th percentiles) of monthly discharge across the 2002–2021 period: **b**, Ganges River; **c**, Sabarmati River; **d**, Ziya River; **e**, Lower Yellow River; **f**, Indus River; **g**, Mekong Delta; **h**, Iran Central Plateau; **i**, Upper Tigris–Euphrates, **j**, California Central Valley; and **k**, Lower Tigris–Euphrates. Basemap data in **a** from Esri, Garmin International, Inc., the US Central Intelligence Agency (The World Factbook) and the National Geographic Society.